Waste Management 190 (2024) 24–34

Contents lists available at ScienceDirect

Waste Management

journal homepage: www.elsevier.com/locate/wasman

Research Paper

Effect of thermochemical treatment of sewage sludge on its phosphorus leaching efficiency: Insights into leaching behavior and mechanism

Tan-Phat Vo [a], Ruichi Zhang [a], Jukka Rintala [a], Keke Xiao [b], Chao He [a,*]

[a] Materials Science and Environmental Engineering, Faculty of Engineering and Natural Sciences, Tampere University, Tampere, Finland
[b] Environmental Science and Engineering Program, Guangdong Technion – Israel Institute of Technology, 241 Daxue Road, 515063 Shantou, Guangdong, China

ARTICLE INFO

Keywords:
Sewage sludge
Hydrochar
Biochar
Incinerated ash
Phosphorus extraction
Leaching kinetics

ABSTRACT

Thermochemical conversion, including hydrothermal processing, pyrolysis and incineration, has become a promising technology for sewage sludge (SS) treatment and disposal. Furthermore, acid leaching is considered as an effective method to recover phosphorus (P) from SS and its thermochemical treatment products. This study has investigated the potential of P reclamation from SS and its thermochemical derivatives, including hydrochar (HC), biochar (BC), and SS incinerated ash (SA). Comparative analyses of physicochemical properties of these derivatives revealed a decrease in hydroxyl and aromatic groups and an increase in aliphatic and oxygen-containing functional groups in HC and BC. Leaching experiments using 1 M sulfuric acid (H_2SO_4) and 1 M oxalic acid ($C_2H_2O_4$) suggested that H_2SO_4 slightly outperformed $C_2H_2O_4$ in terms of P leaching efficiency. HC achieved 79.1 % optimal leaching efficiency in 60 min using H_2SO_4, while BC, SS, and SA required 360 min to achieve comparable efficiency. SS and BC reached optimal leaching efficiency at 74.1 % and 76.2 % in H_2SO_4, while SA achieved 80.9 % in $C_2H_2O_4$. Importantly, HC and SA are more favorable for P extraction using acid leaching, whereas BC tends to be a potential P carrier. Time-dependent kinetics revealed a two-stage leaching process, i.e., fast and slow reaction stages. Shrinking core model indicates product layer diffusion as the primary rate-limiting step in both stages. Overall, these fundamental insights play an important role in practical P recovery through acid leaching of SS derived residues after thermochemical treatment.

1. Introduction

Phosphorus (P) is an indispensable element for all life forms and possesses irreplaceable importance, particularly in the global food production sector, which heavily relies on fertilizers derived from phosphate rocks (Meng et al., 2019). As a primary source of P for fertilizer production, nonrenewable P rock reservoirs are predicted to be depleted within a century (Mew, 2016). Consequently, P has been listed as a critical material by the European Commission (European Commission et al., 2023), highlighting the urgent need for its retrieval from P-bearing waste materials (Wang et al., 2018). Among all biomass wastes, sewage sludge (SS) from wastewater treatment plants contains the highest P concentrations (Jupp et al., 2021), making it a promising and significant source for P recovery.

Recently, various thermochemical technologies have been employed to address SS concerns and facilitate P recovery from SS-derived products. These alternatives, including hydrothermal processing (HTP), pyrolysis and incineration, have emerged as viable options compared to traditional disposal methods. They offer notable advantages, such as odor elimination, enhanced efficiency, considerable waste volume reduction (approximately 90 %), the destruction of organic pollutants, and deactivation of pathogens (Liang et al., 2019; Liu et al., 2021a; Meng et al., 2019). In HTP, the distribution of P within the hydrochar (HC) ranging from 4 % to 13 %, comparable to low-grade phosphate rock with an approximate P content of 8 % (Liu et al., 2021a). In pyrolysis and incineration, P becomes concentrated in biochar (BC) and sludge ash (SA). The content of P in ash is 5–11 % (maximum concentration is up to 20 %) (Meng et al., 2019). Thermochemical treatments influence not only P concentration in the end products but also modify speciation of P in SS, which might cause an impact on P recovery methods. Therefore, understanding the evolution of P species in SS during thermochemical treatment is essential for developing effective SS management and P recovery strategies.

Wet chemical methods have gained prominence for P extraction from SS, HC, BC and SA due to their operational simplicity and cost effectiveness (Kleemann et al., 2017; Liang et al., 2019; Shiba and Ntuli, 2017; Waldmüller et al., 2021). Leaching agents, including inorganic

* Corresponding author.
E-mail address: chao.he@tuni.fi (C. He).

https://doi.org/10.1016/j.wasman.2024.09.004
Received 11 April 2024; Received in revised form 16 August 2024; Accepted 6 September 2024
Available online 11 September 2024
0956-053X/© 2024 The Author(s). Published by Elsevier Ltd. This is an open access article under the CC BY license (http://creativecommons.org/licenses/by/4.0/).

Nomenclature

Aal	Aliphatic
Aar	Aromatic
$A_{C=O}$	Abundance of oxygen functional groups
BC	Biochar
FTIR	Fourier Transform Infrared Spectroscopy
HC	Hydrochar
HTP	Hydrothermal processing
P	Phosphorus
SA	Sludge ash
SCM	Shrinking core model
SS	Sewage sludge

acids, organic acids, alkali, and chelating agents, have been widely employed (Liang et al., 2019; Petzet et al., 2012; Stark et al., 2006; Waldmüller et al., 2021). Inorganic acids, particularly sulfuric acid (H_2SO_4), are notable for their cost-effectiveness and high P leaching efficiency, exceeding 80 % from SS, HC, BC and approximately 100 % from incinerated SA (Table S1) (Liang et al., 2019; Shiba and Ntuli, 2017; Waldmüller et al., 2021). While oxalic acid ($C_2H_2O_4$) is recognized as a potent organic acid, the literature regarding its efficacy in P recovery from leaching solutions remains sparse. Predominantly, $C_2H_2O_4$ has been utilized for P leaching from incinerated SA (Table S1) (Atienza–Martínez et al., 2014; Fang et al., 2018; Liang et al., 2019). Consequently, there is a critical need to investigate the effects of $C_2H_2O_4$ on P leaching from various forms of SS, including original SS, HC and BC.

Previous investigations have primarily focused on the wet-chemical extraction of P from individual thermochemical SS-derived products, providing valuable insights into P behavior under varying conditions (Kleemann et al., 2017; Liang et al., 2019; Shiba and Ntuli, 2017; Waldmüller et al., 2021). However, the literature lacks comprehensive studies in comparing P transformation and recovery mechanisms across SS and its thermal derivatives, such as HC, BC and SA. The efficacy of P reclamation methods for specific SS-derived thermal products remains a topic of ongoing debate. This knowledge gap emphasizes the necessity for developing optimized, substrate-specific P recovery strategies for diverse SS-derived materials. Additionally, variations in SS origin may affect P-leaching behaviors, further emphasizing the need for a comprehensive understanding to guide the selection of suitable thermochemical technologies for various SS types.

This study is the first attempt to holistically assess the effects of thermochemical treatments on the chemical composition of SS-derived products (e.g., HC, BC and SA) with a focus on understanding their influence on P leaching efficiency. A consistent SS source is used in this work to enable precise correlation and comparison of P leaching behaviors after different thermochemical treatments. In particular, SS, HC, BC and SA will be examined as individual P sources in leaching experiments with varied contact times using two typical leaching agents (e.g., H_2SO_4 and $C_2H_2O_4$). The main objectives are to 1) reveal the effects of different thermochemical treatment processes on the physicochemical properties of SS-derived products and especially the subsequent P leaching performance; 2) evaluate comprehensive P leaching efficiency and behaviour under varied leaching conditions to identify the most promising practice for P leaching and reclamation during thermochemical conversion of SS; and 3) ultimately elucidate the P leaching mechanism through kinetics analysis and model validation to achieve more efficient P leaching. This study provides fundamental information and insights to deploy practical strategies to integrate effective P recovery with thermochemical treatment of SS.

2. Materials and methods

2.1. Materials

SS used in this study was collected from Viinikanlahti Wastewater Treatment Plant located in Tampere, Finland, where approximately 33 million m^3 of wastewater was treated annually and ferric sulphate was used as coagulant. The generated SS was subjected to anaerobic digestion followed by dewatering process. The collected SS was then stored in a cold room (4 °C) until further use.

2.2. Thermochemical treatment experiments

HTP, pyrolysis and incineration were conducted at 250, 350 and 550 °C. The selection of temperatures was made to facilitate a reasoned comparison across these thermochemical treatments. This approach allows for the evaluation of how different temperatures, correlating to varying levels of energy consumption, influence the efficiency and product characteristics of each process. Particularly, HC was produced by a HTP in a 2 L Parr® 4500 pressure reactor with an external circulating cooling water system. The procedure commenced by loading 1000 g of dried SS and 600 mL of Milli-Q water into the reactor. Nitrogen gas was subsequently introduced for purging purposes. The reactor was then heated and held at 250 °C for a retention time of 30 min and internal rotary mixer (initially 200 rpm). Eventually, the produced HC was separated from the reaction mixture through vacuum filtration with a 100 μm stainless steel mesh and subjected to drying at 105 °C for 24 h. BC was obtained through a pyrolysis process employing a 10 L stainless steel vessel (31 cm length and 22 cm outer diameter). In this process, 1000 g of dried SS was loaded into the reactor and pyrolyzed at 350 °C in an electrically powered oven for a treatment time of 1 h, with continuous purging of nitrogen gas. SA was produced by incineration of 1000 g of dried SS in a muffle furnace operating at 550 °C for a retention time of 2 h. The schematic diagram of the experiments can be found in Fig. 1.

2.3. Acid leaching experiments

2.3.1. Leaching procedure

Leaching experiment was conducted using SS, HC, BC, and SA. To ensure consistent interaction with the leaching reagent, all samples were initially manually ground to a uniform size of < 200 μm. Subsequently, 1 g of each sample and 20 mL of leaching reagents, including 1 M H_2SO_4) and 1 M $C_2H_2O_4$, were loaded into a 50 mL Falcon tube. The mixture was then shaken at room temperature (25 °C) for varying leaching times (0, 2, 5, 10, 15, 30, 60, 360, 1440 min). Afterward, solid residues and leachate were separated through vacuum filtration using a 2 μm filter paper, and both components were preserved for further analysis (Fig. 1).

The P leaching efficiency was calculated by the following Eq. (1).

$$P_e(\%) = \frac{P_{Ct}}{P_{Ci}} \times 100\% \quad (1)$$

where P_e is the leached efficiency (%); P_{Ct} is the P concentration at the t time (mg/g); P_{Ci} is the P concentration in an initial sample (mg/g).

2.3.2. Phosphorus leaching kinetics

The leaching experimental data was fitted with second-order kinetics to investigate leaching behavior of different samples. The second-order leaching model is shown in Eq. (2). With the boundary condition t = 0 to t give the integration of the differential equation Eq. (3) (Ho et al., 2005).

$$\frac{dC_t}{dt} = k(C_s - C_t)^2 \quad (2)$$

$$C_t = \frac{C_s^2 kt}{1 + C_s kt} \quad (3)$$

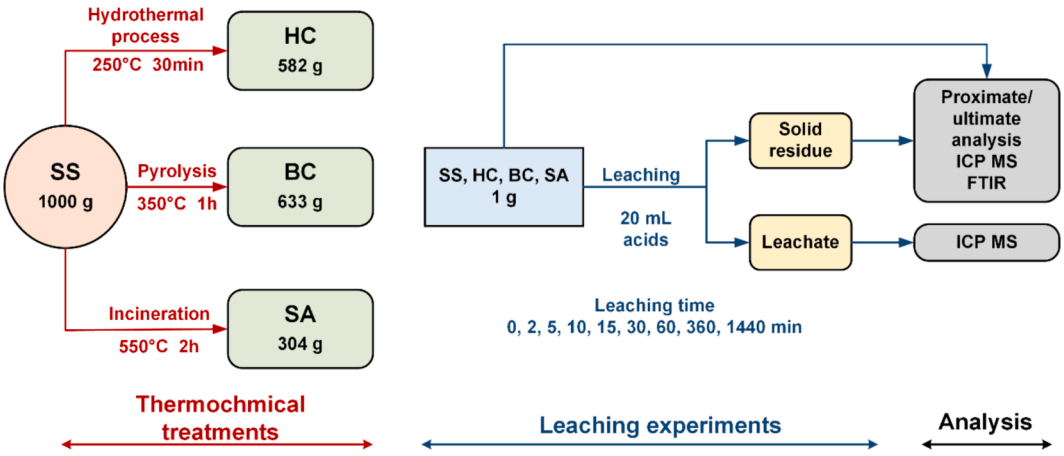

Fig. 1. The schematic diagram of experiments.

where k is the second-order leaching rate constant (L/g/min); C_s is the saturation capacity (g/L); C_t is the concentration of the respective element in the leachate at time t (min). To investigate the two-stage leaching mechanism further, the experimental data were fitted with shrinking core model (SCM) using Eqs. (4) – (6) (Liu et al., 2021b). This model elucidates a heterogeneous solid–liquid reaction, typically governed by either diffusion or chemical reaction kinetics. It describes the leaching agent diffusing through a liquid film surrounding the particle, passing through the solid product layer, and reacting at the surface of the unreacted core.

$$X = k_F t \quad (4)$$

$$1 - 3(1 - X)^{2/3} + 2(1 - X) = k_P t \quad (5)$$

$$1 - (1 - X)^{1/3} = k_R t \quad (6)$$

where X is the leaching efficiency at a given time t (min); k_F, k_R and k_P are rate constants for each leaching step liquid film diffusion, chemical reaction and product layer diffusion, respectively. To predominant rate-limiting step is determined by best linear correlation with highest the correlation coefficient (R^2).

2.4. Analytical methodologies

The elemental composition (C, H, N, and S) of the SS, HC, BC and SA samples was determined using a Thermo Scientific FlashSmart elemental analyzer (CHNS/O). ASTM methods (D3173–11, D3174–11, and D3175–11) were used to determine the moisture, ash and volatile matter contents in SS, HC, BC and SA. Element concentrations in solid samples (0.5 g) and leachates (1 mL) were determined using inductively coupled plasma mass spectrometry (Thermo Scientific iCAP™ RQ) equipped with a concentric Nebulizer after microwave digestion in 5 ml hydrogen peroxide (30 % solution) and 5 mL nitric acid (65 % solution). The functional groups of SS, HC, BC and ash were detected by using a Fourier transform infrared spectroscopy (FTIR) (Spectrum Two FT-IR Spectrometer L1600300). The instrument was operated in single reflection mode with a speed of 5 kHz, a resolution 4 cm and a mid-IR range of 600 and 4000 cm^{-1}.

3. Results and discussion

3.1. Physicochemical properties of sewage sludge and derived thermochemical products

The physicochemical properties of SS can be altered during thermochemical treatments. Consequently, the properties of SS change in terms of volatile matter, elemental composition, mineral content, and functional groups, thereby influencing the characteristics and potential applications of the derived products. The changes in these properties are discussed in detail as below.

3.1.1. Proximate and ultimate analysis

The fixed carbon (2.3 %), ash content (46.9 %) and volatile matter (50.8 %) in SS exhibited an increment by 3.4 % and 48.1 % in HC and 4.0 % and 52.5 % in BC after HTP and pyrolysis respectively, while the volatile matter (50.8 %) in SS decreased by 48.4 % in HC and 43.5 % in BC as shown in Table 1. During HTP, the variation of fixed carbon and volatile matter could be attributed to the following pathways (1) volatile matter initially decomposes, yielding volatile gases and soluble intermediates in the gas and liquid phases, respectively and (2) the soluble intermediates contribute to an increase of fixed carbon through carbonization and condensation processes on the surface of HC (He et al., 2016; Yang et al., 2023; Zhuang et al., 2019). Similarly, during pyrolysis, the volatile matter released due to the devolatilization into intermediates and char, while fixed carbon indicates solid combustible

Table 1
Main characteristics of SS and derived thermochemical products.

		SS	HC	BC	SA
Proximate analysis (wt%)	FC [a]	2.3 ± 0.2	3.4 ± 0.2	4.0 ± 1.1	–
	VM	50.8 ± 1.7	48.4 ± 1.8	43.5 ± 2.8	–
	Ash	46.9 ± 1.5	48.1 ± 0.5	52.5 ± 2.9	–
Ultimate analysis (wt%)	C	26.1 ± 0.8	27.3 ± 1.9	25.6 ± 1.5	–
	H	5.1 ± 0.2	4.6 ± 0.5	3.6 ± 0.7	–
	N	3.6 ± 0.7	2.4 ± 1.1	3.2 ± 0.9	–
	S	0.5 ± 0.1	0.5 ± 0.2	0.6 ± 0.1	–
	O [b]	17.9 ± 1.1	17.0 ± 0.5	14.5 ± 1.1	–
Major elements (mg/g)	P	22.4 ± 2.5	26.7 ± 2.5	33.5 ± 2.8	56.5 ± 3.5
	Ca	37.1 ± 4.8	44.6 ± 5.5	44.3 ± 6.1	100.1 ± 6.8
	Mg	1.6 ± 0.5	1.8 ± 0.1	1.8 ± 0.3	4.4 ± 1.2
	Al	7.7 ± 1.8	9.4 ± 1.2	11.7 ± 2.1	20.6 ± 1.5
	Mn	0.4 ± 0.1	0.4 ± 0.1	0.4 ± 0.1	1.1 ± 0.1
	Fe	87.7 ± 10.7	111.2 ± 9.8	113.8 ± 18.9	204.3 ± 32.2

Note:
–, not applicable.
VM: volatile matter, FC: fixed carbon.
[a] Calculated by difference using 100 %−VM%−Ash%.
[b] Calculated by using 100 % −C%−H%−N%−S%−Ash%.

residue left over after the complete burning and releasing of volatiles (Gao et al., 2020; Kan et al., 2016). Additionally, the increase in ash content in both HC and BC could be attributed to the decomposition of most volatile matters into gas and liquid phases (Fan et al., 2020; Yang et al., 2023).

C content increased to 27.3 % in HC and 25.6 % in BC compared to SS (26.1 %). Conversely, H and O contents experienced consistent decreases after thermochemical treatments (Table 1). The observed changes in C, H, and O consequently influenced the H/C and O/C ratios, decreasing HC and BC relative to SS (Fig. S1). The changes in the H/C and O/C ratios were induced by decarboxylation and dehydration reactions occurring during HTP and pyrolysis (Wang et al., 2019; Yang et al., 2023). Notably, the H/C ratio in HC is higher compared to BC, whereas the O/C ratio in BC exceeds that of HC (Fig. S1). Tang et al. (2019) reported that H/C and O/C ratios represent the degree of aromaticity and polarity; furthermore, low H/C and O/C ratios indicated more aromatic and less hydrophilic surfaces. Results suggest that BC has a less aromatic and more hydrophobic surface than HC (Fig. S1) (Suggate and Dickinson, 2004).

3.1.2. Major element composition

The increased concentrations of P and metals in derived products compared to SS are presented in Table 1. The concentration of P increased from 22.4 mg/g in SS to 26.7, 33.5 and 56.5 mg/g in HC, BC and SA respectively. Similarly, the concentration of other metals exhibited the increment, in which SA obtained the highest concentration followed by BC and HC (Table 1). The increment of concentration is due to the volume reduction after thermochemical processes. Particularly, P is enriched together with metals in HC, BC and SA (Meng et al., 2019; Pérez et al., 2022). The higher temperatures lead to increased metal concentrations remaining in the final solid products (i.e., HC, BC and SA) (Chanaka Udayanga et al., 2018; Januševičius et al., 2022).

During HTP, the presence of Mg, Ca, Fe, and Al in SS can be advantageous for P reclamation due to the dissolution of metals and the destabilization of metal-phosphate bonds (Fang et al., 2018), leading to the retention of P in HC through the formation of insoluble phosphates (Merzari et al., 2020), while the soluble phosphates dissolved into process water (Pérez et al., 2022). Similarly, Ca plays a significant role in forming Ca-P bonding such as whitlockite or hydroxylapatite in pyrolysis (Kleemann et al., 2017). In the case of incineration, Fe and Al are typically bonded with P in SA (Meng et al., 2019). Particularly, the presence of Fe in the ash significantly influences P extraction. Iron phosphate within SS char undergoes oxidation during incineration, resulting in the formation of acid-insoluble iron compounds like hematite and acid-soluble phosphate compounds (Atienza–Martínez et al., 2014).

3.1.3. Evolution of functional groups

To determine the variation of functional groups during thermochemical processes, the FTIR absorption bands were deconvoluted into several sub-peaks (Yang et al., 2023). Particularly, CH_2/CH_3 represents the aliphatic (A_{al}) side chain length and branching degree (Lin and Ritz, 1993), A_{ar}/A_{al} signifies the ratio of aliphatic to aromatic (A_{ar}) hydrocarbons within the coal structure (Suggate and Dickinson, 2004) and $A_{C=O}/A_{ar}$ parameter is indicative of the abundance of oxygen functional groups ($A_{C=O}$) (Qiang et al., 2021) as following Eqs. (8) – (10), respectively.

$$\frac{CH_2}{CH_3} = \frac{I_{2920-2945cm^{-1}}}{I_{2955-2960cm^{-1}}} \quad (8)$$

$$\frac{A_{ar}}{A_{al}} = \frac{I_{700-900cm^{-1}}}{I_{2800-3000cm^{-1}}} \quad (9)$$

$$\frac{A_{C=O}}{A_{ar}} = \frac{I_{1640-1700cm^{-1}}}{I_{1500-1630cm^{-1}}} \quad (10)$$

The absorption intensity of SS and its thermochemical derivatives present four main peaks (Fig. S2), which are related to: Group (1) – the hydroxyl group (3700–3000 cm^{-1}), Group (2) – aliphatic structure (3000–2800 cm^{-1}), Group (3) – oxygen-containing functional group structure (1800–1000 cm^{-1}), and Group (4) – aromatic structure (900–700 cm^{-1}) (Qiang et al., 2021; Wei et al., 2019). After thermochemical processes, the absorption intensity of Group (2) and (3) of HC, BC and SA was relatively strengthened, while it was weakened of Group (1) and (4). The examination of the deconvoluted spectra of SS is discussed in Fig. S3 and Table S2.

The peak fitting of Group (2) in the derived thermochemical products shifted compared to SS (Fig. 2a). Particularly, the appearance of peaks at 2975 cm^{-1} and 2885 cm^{-1} in HC, BC and SA represented to asymmetric and symmetric stretching of CH_3 respectively, while the loss of peaks at 2921 cm^{-1} and 2852 cm^{-1} in BC and SA indicated the loss of asymmetric and symmetric stretching of CH_2 (Table S3) (Lin and Ritz, 1993). Notably, the aliphatic structural regions in HC were indicated by four Gaussian peaks which contrasts with the three peaks observed in SS, BC, and SA, which can be explained that the lengths of the aliphatic chains are reduced with temperature increment. Furthermore, the CH_2/CH_3 ratio increased from 0.2 (SS) to 0.24 (HC), 0.37 (BC), and 0.35 (SA) (Table S4), indicating the cleavage of long aliphatic chains in SS during thermochemical processes (Lin and Ritz, 1993; Yang et al., 2023).

The evolution of oxygen-containing functional group (Group (3) is shown in Fig. 2b. SS exhibits five Gaussian peaks. The number of peaks subsequently increased to nine in HC, seven in BC, and six in ISSC (Table. S3). The increment of Gaussian peak numbers in HC could be attributed to release of C=O functional groups via decarboxylation reactions (Pérez et al., 2022) which was confirmed by the results of the ultimate analysis (Fig. S1). The ratio $A_{C=O}/A_{ar}$ in SS, which stands at 0.4, shows a reduction to 0.35 in HC and 0.32 in BC (Table S4), indicating a transformation of carbonyl or carboxyl groups into aromatic structures (Yang et al., 2023). The findings indicated that HC have more aromatic compounds compared to BC. Lu et al. (2013) reported that the BC becomes recalcitrant when their surface contains aliphatic and aromatic compounds.

Notably, the broad band 1300–800 cm^{-1} represents overlapping vibrations of SiO_2 and PO_4^{3-} compounds (Fig. 2c) (Pérez et al., 2022). Particularly, peaks ranging from 1200–1000 cm^{-1} indicate the amorphous P-bearing compounds (Al-P, Ca-P) (Lee and Kim, 2017). In this study, the P compounds in SS comprised six Gaussian peaks including $Ca_3(PO_4)_2$ (1042 and 1030 cm^{-1}), $AlPO_4$ (1115 cm^{-1}), $Mg_3(PO_4)_2$ (980 cm^{-1}), $H_2PO_4^-$ (940 cm^{-1}), and SiO_2 (1076 cm^{-1}) (Table. S5) (Elzinga and Sparks, 2007; Lee and Kim, 2017; Vogel et al., 2011). After HTP and incineration, the number of compounds remained similar; however, the intensity and numbers of Gaussian peaks exhibited an increment. Pyrolysis indicated the decrement in both intensity and number of Gaussian peaks (Table. S5). The transformation of P and P-bearing compounds during thermochemical processes is going to be discussed in the following section.

3.2. The effect of leaching parameters on phosphorus extraction efficiency

To evaluate the leaching behavior and efficiency of P from SS, HC, BC and SA, a systematic investigation was conducted focusing on the influence of key variables, including the type of leaching solution, the nature of the P source, and the contact time between the materials and the leaching solution. These factors are critical in understanding the release of P from various sources under different conditions.

3.2.1. The effect of acid-leaching solutions

Two different acids (H_2SO_4 and $C_2H_2O_4$) with identical concentration (1 M) were used for comparative P leaching from SS, HC, BC and SA. The concentration of acids was selected based on a previous investigation that 1 M H_2SO_4 was considered as the optimal concentration for P leaching (Shiba and Ntuli, 2017). Possible reactions between inorganic P

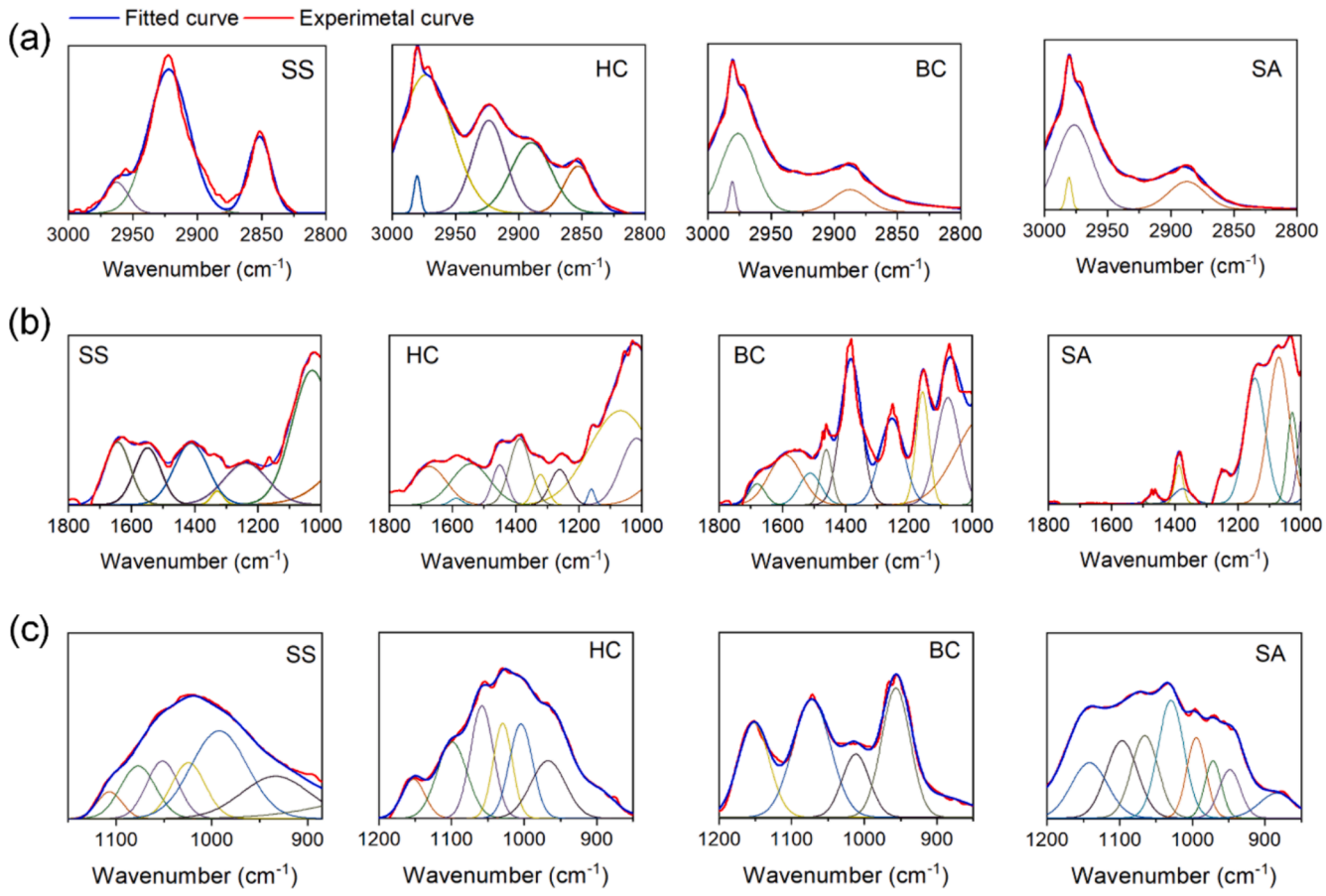

Fig. 2. Comparative fitted curves of FTIR spectra of SS, HC, BC and SA in (a) Group (2) – aliphatic structure (3000–2800 cm^{-1}) and (b) Group (3) – oxygen-containing functional group structure (1800–1000 cm^{-1}) and (c) P-bearing compounds (1200–800 cm^{-1}).

phases with acid are presented in Eqs. (S1) –(S4) (Pérez et al., 2022). The comparative P leaching efficiency from SS, HC, BC and SA using H_2SO_4 and $C_2H_2O_4$ are illustrated in Fig. 3. The results showed that H_2SO_4 outperformed $C_2H_2O_4$ in P leaching efficiency for SS and BC when the contact time exceeded 60 min. Conversely, demonstrating higher efficiency in P leaching within shorter contact times, under 60 min. A similar trend was observed for HC at a 2 min contact time (Fig. 3). The outperformance of $C_2H_2O_4$ at short contact time could be attributed to the lower molecular weight of $C_2H_2O_4$ compared to H_2SO_4, which allows $C_2H_2O_4$ to diffuse more rapidly through the particle matrix, thereby reaching P sites more swiftly. Previous studies have reported the efficacy of H_2SO_4 in P leaching from SS and derived products, in which Shiba and Ntuli. (2017) demonstrated that H_2SO_4 outperformed other inorganic acids such as HCl and HNO_3 in leaching P from SS, with 1 M H_2SO_4 achieving 82 % P leaching efficiency in 120 min. Similarly, Atienza–Martínez et al. (2014) reported that approximately 90 % of P was leached from combustion ash (treated at 900 °C) using H_2SO_4 within the same timeframe.

Noteworthy, $C_2H_2O_4$ demonstrated a greater P leaching efficiency compared to H_2SO_4 for SA, achieving approximately 10 % higher efficiency within a 15-min contact time. However, this efficiency gap narrowed as the contact time increased (Fig. 3). The findings are in line with Liang et al. (2019) that $C_2H_2O_4$ was able to extract 100 wt% of P from the SA samples at temperatures ranging from 600 to 850 °C, while H_2SO_4 showed decreasing P leaching efficiency at higher temperatures. Besides, $C_2H_2O_4$ had a better performance than H_2SO_4 in P leaching from SA (Atienza–Martínez et al., 2014; Fang et al., 2018). In this study, H_2SO_4 was more effective for P leaching from HC, contrasting with its performance for SA in comparison with $C_2H_2O_4$. Despite these variations, the differences in P leaching efficiencies between two acids were minimal, implying the crucial influence of the physicochemical properties of the samples on leaching outcomes.

3.2.2. *The effect of type of P product on leaching efficiency*

The physicochemical characteristics such as physical surfaces, porosity, the immobilization of P, and chemical nature of the P play a crucial role on P leaching efficiency. In this study, at the longest contact time (1440 min), the highest P leaching efficiency, reaching 82.2 %, was achieved using both H_2SO_4 and $C_2H_2O_4$, followed by HC (80.8 % and 80.3 %), BC (80.7 % and 75.2 %) and SS (75.9 % and 64.7 %), respectively (Fig. 3). P leaching efficiency from HC was higher than that from other samples in most cases. The remarkable P leaching performance of HC could be attributed to the chemical interactions between the acids and hydrolysable bonds that transpire during the leaching process (Waldmüller et al., 2021). Besides, the water soluble compounds on HC surface could be already dissolved in process water during HTP, resulting in a scenario where acids primarily engage in inorganic dissolution with minimal interference (Liang et al., 2019; Waldmüller et al., 2021). Besides, the steric hindrance caused by the formation of gypsum crystals and/or acid-insoluble hematite and quartz phases may restrict acids from contacting whitlockite crystals (Donatello et al., 2010). Furthermore, BC exhibited the highest resistance to P leaching using both acids when considering varying contact time. This observation is corroborated by the elemental analysis and FTIR findings discussed earlier, which suggest a decrease in chemical reactivity and an increase in hydrophobicity of BC, making it less amenable to P extraction via acid leaching. In contrast, HC demonstrated enhanced efficiency in P leaching over shorter durations, highlighting its suitability for acid leaching process.

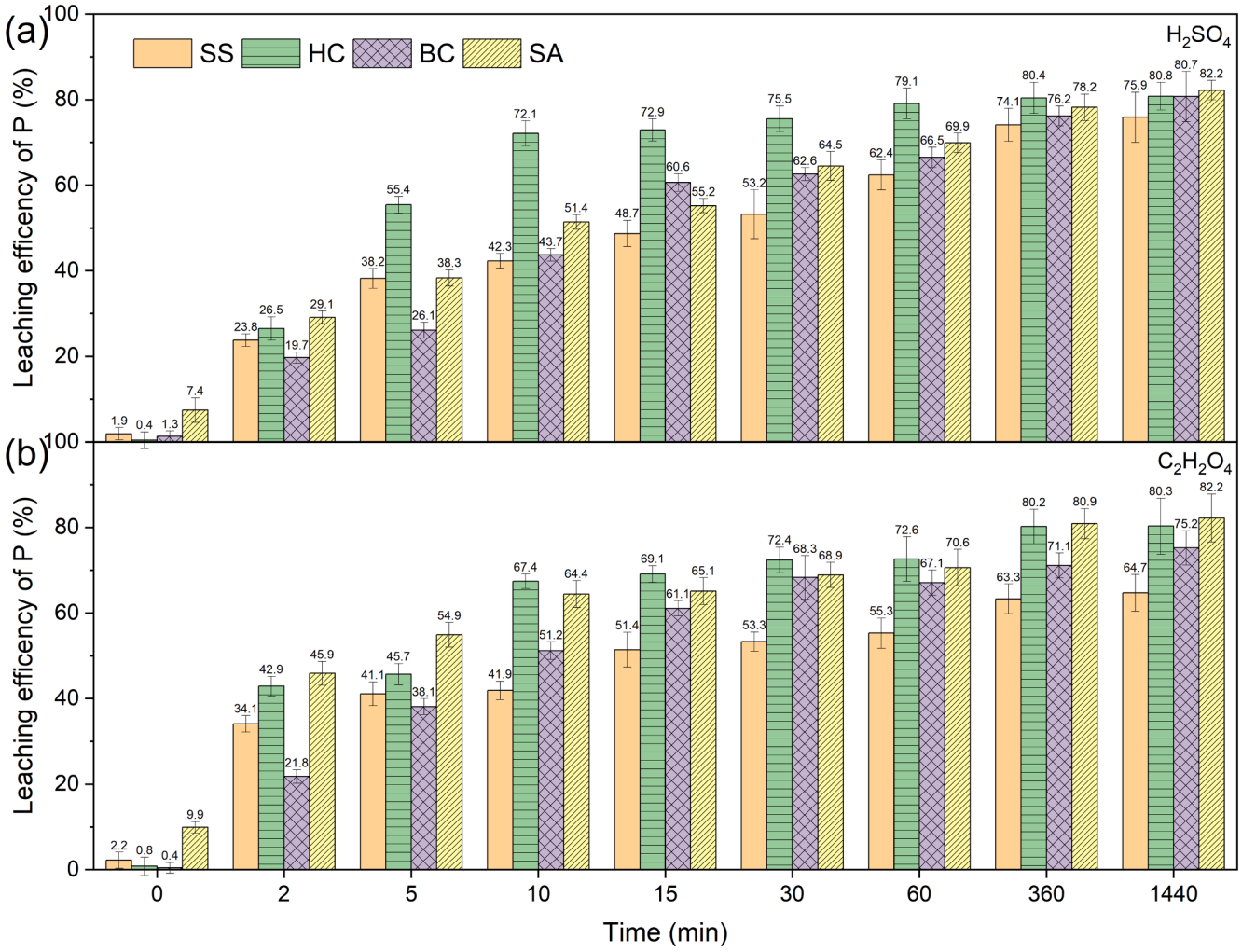

Fig. 3. Comparative P leaching efficiency of SS, HC, BC and SA in (a) H_2SO_4 and (b) $C_2H_2O_4$.

3.2.3. *The effect of contact time*

Extended contact time remarkably enhanced P leaching efficiency in all samples using both H_2SO_4 and $C_2H_2O_4$. However, from an energy consumption perspective, a shorter contact time yielding comparable efficiency (within 10 % difference) is recommended. In this study, HC reached an optimal leaching efficiency of 79.1 % in 60 min with H_2SO_4. In contrast, SS, BC, and SA obtained optimal P leaching efficiency at 360 min, with 74.1 %, 76.2 %, and 80.9 %, respectively (Fig. 3a). In P leaching process, a longer contact time ensures the sufficient leaching of P from the samples into the leachate (Yu et al., 2021). Previous studies have reported that 2 h was the optimal time for P leaching from SS, HC, BC and SA using H_2SO_4 (Atienza–Martínez et al., 2014; Donatello et al., 2010; Kleemann et al., 2017; Liang et al., 2019; Liu et al., 2023; Shiba and Ntuli, 2017). Afterward, P leaching efficiency exhibited negligible increment with the prolonged contact time. The reason could be that there might be other reactions taking place or processes such as crystallization and precipitation of insoluble compounds such as iron phosphates thus forming chemical bonds which are harder to break (Stark et al., 2006). Another possible reason could be that particles tend to adsorb charged ions, leading to surface charges affecting the rheological behavior of the sludge in the leachate (Shiba and Ntuli, 2017).

3.3. *Phosphorus leaching mechanism*

To further understand the leaching dynamics of P from SS, HC, BC and SA, the leaching kinetics were analyzed using both the second-order kinetics model and the SCM. The second-order kinetics model provides insights into the reaction rate with time dependency, offering a detailed understanding of the interactions between the leaching solution and the solid samples. On the other hand, the SCM can elucidate the physical and chemical processes governing the leaching behavior and the controlling mechanisms.

3.3.1. *Second-order kinetics*

The second-order leaching kinetics revealed a distinct pattern in the leaching of P as shown in Fig. 4. The goodness of fit expressed ($R^2 > 0.93$ and $p < 0.05$) with uncertainty analysis for all samples, indicating the suitability of the model (Table 2). Notably, when using $C_2H_2O_4$, all samples exhibit higher k values compared to H_2SO_4 (Table 2), revealing that $C_2H_2O_4$ promotes a faster leaching rate, which explains the above hypothesis of $C_2H_2O_4$ rapid diffusion through the particle matrix. The leaching constant k represents the rate at which the leaching process occurs, indicating how the concentration of soluble compounds in the suspension changes over time (Ho et al., 2005). H_2SO_4 demonstrates superior P leaching efficiency to $C_2H_2O_4$, as evidenced by higher saturation capacity C_s values (Ho et al., 2005). For instance, C_s of P in SS using H_2SO_4 is 0.7 g/L compared to 0.6 g/L with $C_2H_2O_4$, with corresponding leaching time of 6 h and 1 h, respectively. This means H_2SO_4 remains active in leaching P for up to 6 h, while $C_2H_2O_4$ is effective for 1 h (Table 2). Consequently, H_2SO_4 can extract more P over a longer period, leaving less residual P in the SS. In contrast, although $C_2H_2O_4$ has a faster initial leaching rate due to a higher k value, its lower C_s and

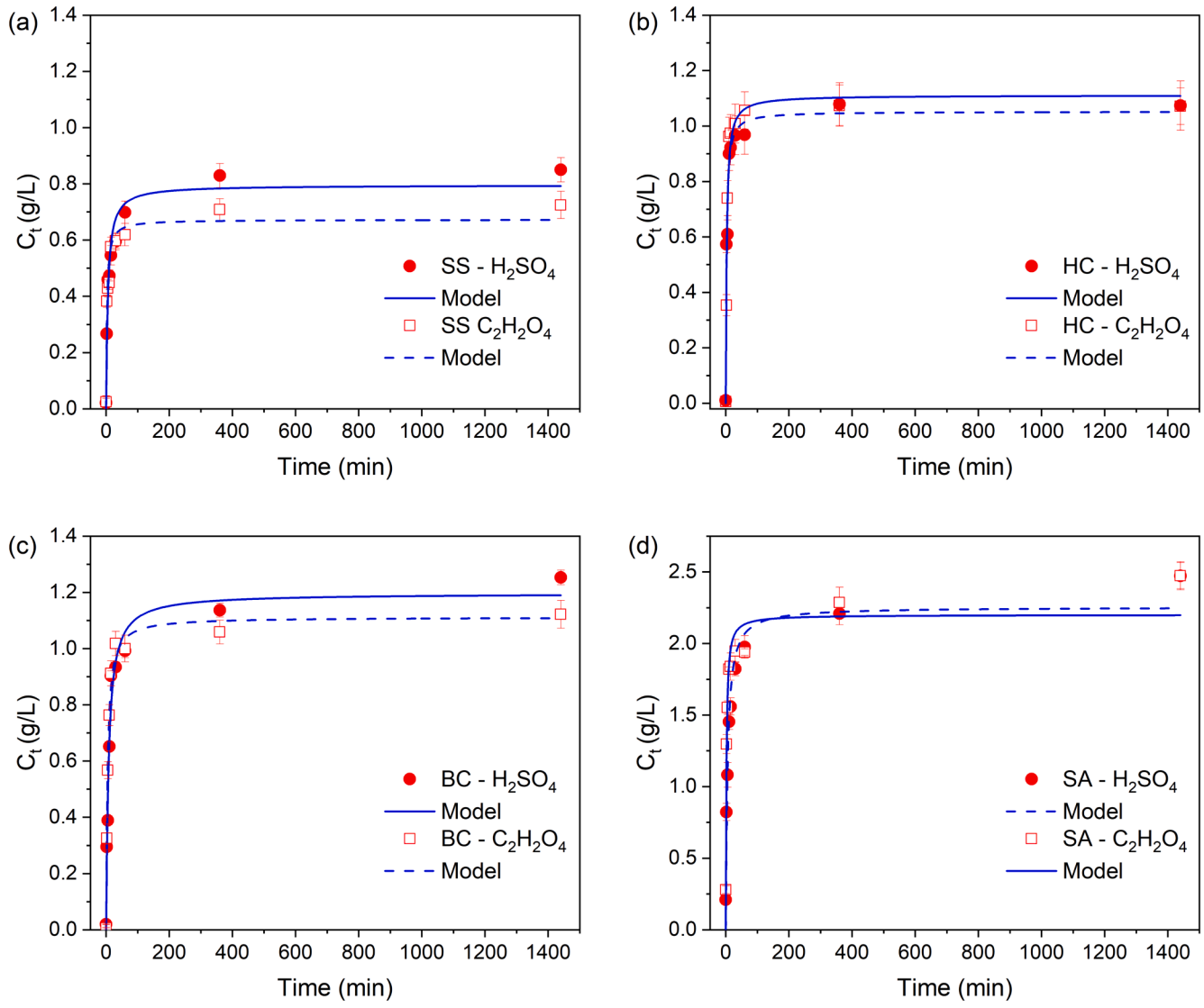

Fig. 4. Second-order kinetics of P leaching from (a) SS, (b) HC, (c) BC and (d) SA in H_2SO_4 and $C_2H_2O_4$.

Table 2
Leaching kinetic parameters of second order and two-phase exponential decay function with 95% confidence intervals for SS, HC, BC and SA in H_2SO_4 and $C_2H_2O_4$.

Second–order kinetics				**Two-phase exponential decay function**		
Sample	**Parameters**		R^2	**Parameters**		R^2
	k (L/g/min)	**Cs (g/L)**		**k1 (1/min)**	**k2 (1/min)**	
SS-H_2SO_4	0.233 ± 0.057	0.795 ± 0.036	0.955	0.548 ± 0.071	0.038 ± 0.017	0.997
SS-$C_2H_2O_4$	0.589 ± 0.177	0.672 ± 0.029	0.941	107.979 ± 1.532	0.119 ± 0.142	0.953
HC-H_2SO_4	0.320 ± 0.057	1.110 ± 0.036	0.977	0.502 ± 0.171	0.402 ± 0. 247	0.998
HC-$C_2H_2O_4$	0.421 ± 0.058	1.052 ± 0.038	0.973	39.578 ± 3.574	0.157 ± 0.120	0.985
BC-H_2SO_4	0.107 ± 0.019	1.196 ± 0.043	0.976	52.181 ± 4.292	0.135 ± 0.219	0.991
BC-$C_2H_2O_4$	0.203 ± 0.022	1.111 ± 0.021	0.992	0.701 ± 0.127	0.187 ± 0.017	0.999
SA-H_2SO_4	0.082 ± 0.019	2.254 ± 0.095	0.956	1.239 ± 0.809	0.127 ± 0.020	0.998
SA-$C_2H_2O_4$	0.246 ± 0.081	2.200 ± 0.096	0.925	27.459 ± 1.786	0.160 ± 0.200	0.967

shorter effective period limit its overall P extraction.

The second-order leaching kinetics of P also revealed a biphasic process consisting of a fast reaction stage followed by a slower reaction stage for SS, HC, BC and SA. The application of a two-phase exponential decay function on rate of concentration change (dC_t/dt) was calculated by Eq. S5, showing an excellent fit ($R^2 > 0.95$ and $p < 0.05$) for all samples (Table 2). Noteworthy, the results indicate that k1 > k2 in all samples and conditions (Table 2), signifying that the initial stage exhibits a faster rate compared to the subsequent stage. It is postulated that in the fast reaction stage, P rapidly dissolves into the leaching solution due to the high solubility of certain phosphates, leading to a significant release of P. In the slow reaction stage, increased dissolved salt concentrations reduce the concentration gradient, slowing P diffusion and decreasing the leaching rate over time. The transition from the fast reaction stage to the slower reaction stage in the biphasic leaching process could be influenced by several factors such as surface reaction

and diffusion control, particle size and porosity, or the solubility of P in the samples. This hypothesis will be validated using the shrinking core model. The observed kinetics align with the findings reported by Li et al., 2021. Their study demonstrated that P leaching from phosphate ore using phosphoric acid exhibits a biphasic process with distinct fast and slow reaction stages. The fast reaction stage occurred within the initial three minutes of the process. It is important to note that the duration of these fast and slow reaction stages can vary significantly, depending on multiple factors (e.g., the nature of the P source, leaching conditions, leaching agents) (Faraji et al., 2022).

3.3.2. *Shrinking core model*

The SCM was applied to elucidate the rate-limiting steps in the leaching process (Fig. 5), including liquid film diffusion, solid product layer diffusion, and chemical reaction across SS, HC, BC, and SA, using H_2SO_4 and $C_2H_2O_4$. As detailed in Table S6, a comparative assessment of k and R^2 indicates product layer diffusion as the predominant control step, as evidenced by the highest R^2 in this category (Table S6). Furthermore, the results revealed that the rate constant k_F was the highest among all samples for both H_2SO_4 and $C_2H_2O_4$, followed by k_R and k_P (Table S6). If one of these steps is significantly slower than the others, it becomes the rate-controlling step in the leaching process (Faraji et al., 2022). A higher rate constant indicates a more rapid progression of the respective step, suggesting that during leaching, the acid solution predominantly diffuses through the liquid film surrounding the particle. Subsequently, a chemical reaction occurs, targeting acid-soluble compounds and phosphate on the surface. The process eventually becomes constrained by diffusion through the product layer, signifying a sequential transition from liquid film diffusion to chemical reaction, and finally to product layer diffusion as the rate-limiting step.

The imposition of product layer diffusion as a rate-limiting step in the fast reaction stage can be ascribed to several factors: (1) its formation creating a barrier that impedes the access of leaching agent to the core and slows P release (Liu et al., 2023); (2) surface reactions initially quick, becoming secondary as diffusion through the layer dictates the reaction pace (Li et al., 2021); and (3) a reduced reaction surface area over time, transitioning the control from surface reactions to diffusion through the product layer (Ray and Ray, 2018). To overcome the product layer, methods should focus on reducing the thickness or improve the porosity of the product layer, or use leaching agents that can penetrate the product layer more effectively (Ray and Ray, 2018). Conversely, when chemical reaction control is identified, optimization should involve changing temperature, concentration of leaching agents, or agitation to enhance the reaction rate (Faraji et al., 2022). Therefore, SCM results help identify the rate-controlling step in the leaching process. Once the controlling process is known, such as chemical reaction, product layer diffusion, or another mechanism, leaching conditions can be optimized by selecting the most effective leaching agents accordingly (Faraji et al., 2022; Ray and Ray, 2018). Moreover, similar observations were reported by Liu et al. (2023) in their investigation of P leaching from HC using HNO_3 that the dominance of product layer diffusion over liquid film diffusion and chemical reaction was the principal rate-limiting mechanism. This dominating step of product layer diffusion was also in good agreement with previous studies that conducted P leaching from phosphate rock using H_2SO_4 (Liu et al., 2021b), rice husk ash by HCl (Wang et al., 2017), and dephosphorization slag by HCl (Du et al., 2020).

The two-stage process (fast and slow reactions) of P leaching is illustrated in Fig. 6. The fast reaction stage is initiated by the diffusion of acid (H^+) through the liquid film enveloping the particles (Diffusion), rapidly reacting with surface P-bearing compounds to release phosphates and metals (Reaction) (Du et al., 2020; Liu et al., 2023). The soluble reaction products efficiently diffuse through the formed product layer and then rapidly through the liquid film into the solution (Migration). This stage is marked by an accelerated leaching rate, facilitated by the high solubility of specific phosphate forms and the effective penetration of the acid. Afterward, as the reaction proceeds, it evolves into a slow reaction stage, where the presence of elevated concentrations of dissolved salts reduces the concentration gradient crucial for P diffusion into the solution (Li et al., 2021; Liu et al., 2023). This reduction in gradient decelerates the mass transfer rate, contributing to a slowdown in the leaching rate. The process gradually shifts towards the center of the particles (i.e., penetration), transitioning from a phase dominated by rapid surface reactions and diffusion through the liquid film to a diffusion-controlled stage hindered by the resistance of the product layer (Fig. 6).

This study demonstrated the P leaching mechanism using second-order kinetics and SCM, both of which showed a very good fit with high R^2 values. While model fitting provides valuable information, it is important to recognize that theoretical leaching kinetics models have limitations. Models often assume uniform particle size, constant temperature, or specific reaction kinetics, which may not hold true in real-world scenarios, potentially leading to misinterpretations. To accurately determine leaching mechanisms, comprehensive analytical characterization techniques are crucial (Faraji et al., 2022). For instance, methods for identifying chemical and structural changes, as well as revealing morphological changes, should be considered to provide direct evidence and detailed insights. These techniques complement theoretical models and ensure a comprehensive understanding of the leaching process. Therefore, integrating model fitting with other analytical methods is essential for drawing accurate conclusions about the leaching mechanisms.

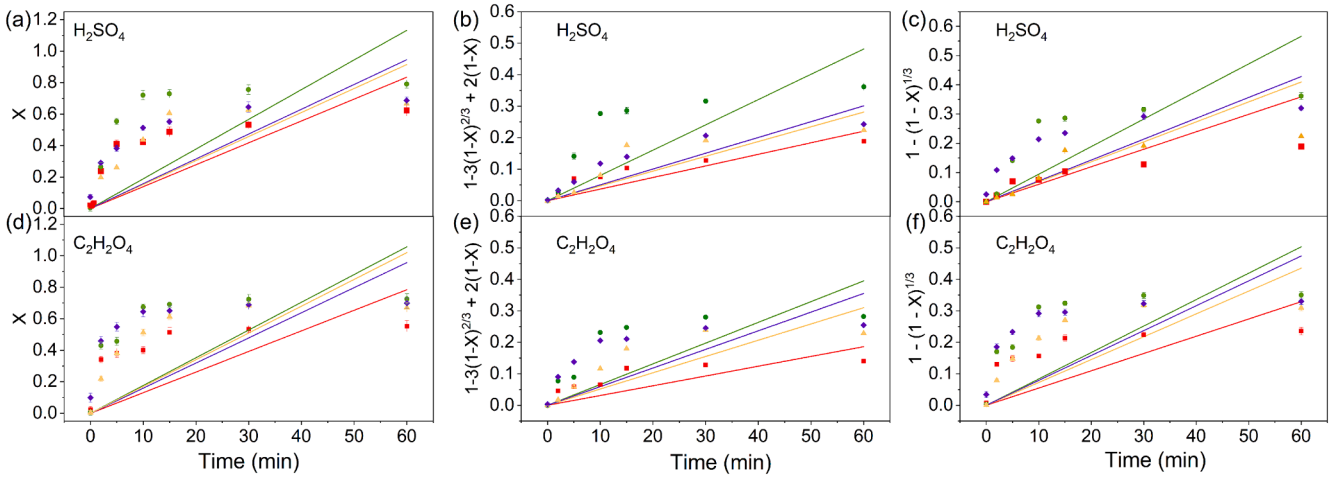

Fig. 5. The correlation of liquid film diffusion, product layer diffusion, and chemical reaction and leaching time for SS, HC, BC and SA.

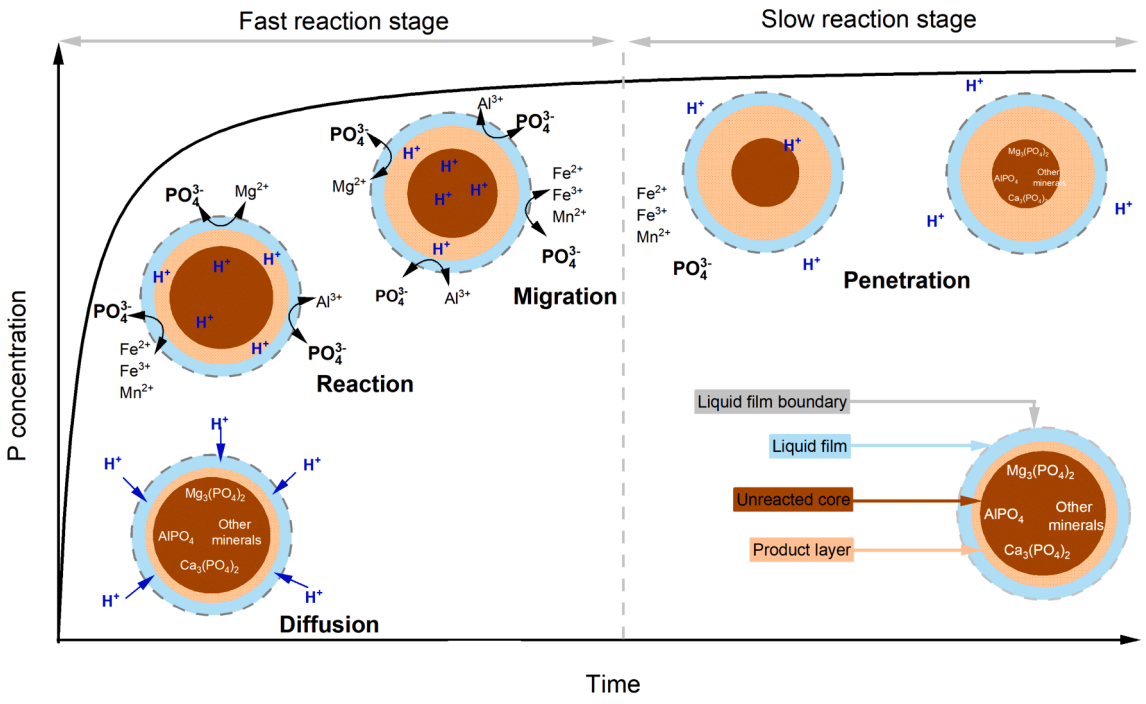

Fig. 6. The two-stage P leaching from SCM of SS, HC, BC and SA.

3.4. *Future perspectives and implications*

The present study marks the initial step in P reclamation via the leaching process by identifying an appropriate thermochemical treatment. Particularly, HC exhibited the highest efficiency and time effectiveness compared to the original SS, BC and SA. Future work should focus on enhancing P recovery by optimizing operational conditions or adding catalysts during treatment. For instance, incorporating organic acid additives in HTP can convert insoluble phosphates into soluble forms, increasing P recoverability from SS (Pérez et al., 2022). Besides, due to containing high concentrations of contaminants (e.g., heavy metals, microplastics, pharmaceuticals), HTP must be carefully studied to ensure effective P recovery while mitigating pollutants without generating additional hazards. Optimizing leaching efficiency by investigating leaching parameters, reducing the thickness or improving the porosity of the product layer, or using leaching agents capable of penetrating the product layer more effectively is also crucial (Lv et al., 2022; Ray and Ray, 2018). Selecting suitable methods for P recovery, such as precipitation, adsorption, or ion exchange (Bouaouda et al., 2023) and conducting an overall energy balance, techno-economic, and life cycle assessments of an integrated system for the entire process (Aghbashlo et al., 2022) are essential steps.

Additionally, the recovery of dominant metals during P recovery should be considered, as different P-bearing compounds have various applications. High concentrations of Fe-P-containing products could be synthesized into $LiFePO_4$ for lithium batteries (Hu et al., 2023). Meanwhile, high concentrations of Ca-P and Al-P, coupled with struvite, could be utilized for fertilizer production (Zhang et al., 2020). However, potential environmental risks should be considered when recovering P as a fertilizer from SS sources due to the presence of harmful substances (Lamastra et al., 2018). Despite the promising results, further research and pilot studies are necessary to fully assess the industrial feasibility and sustainability of these processes, taking into account environmental impact, regulatory compliance, and economic viability.

4. Conclusions

Acid leaching is an effective approach for P recovery from SS and its thermochemical products. This study has investigated the influence of various thermochemical processes on the evolution of physicochemical properties and P leaching behavior of solid products (i.e., HC, BC, and SA). Among all tested samples, HC demonstrated the highest optimal P leaching efficiency of 79.1 % by H_2SO_4 within 60 min. After 360 min, P leaching efficiency using H_2SO_4 for SS and BC was 74.1 % and 76.2 %, respectively, while 80.9 % of P leaching efficiency was obtained for SA by using $C_2H_2O_4$. HC was found to be the most favorable for P leaching with BC being the least one. SA showed good P leaching efficiency, especially when $C_2H_2O_4$ was used. Although P leaching efficiency using H_2SO_4 for SA was not that high, significant P can still be extracted, making it a viable option for P recovery by selecting an appropriate leaching agent. Given the lower energy consumption for HTP than incineration, HC may be superior material to SA for P leaching. In spite of 5 % lower P leaching efficiency than using H_2SO_4, $C_2H_2O_4$ promoted the faster leaching in the initial one hour. Thus, combined HTP and sequential $C_2H_2O_4$ leaching of HC suggests great potential for P recovery from SS in industrial applications. Furthermore, leaching kinetics revealed a two-stage behavior of P leaching for all samples, including a fast reaction stage and a slow reaction stage. The SCM was successfully applied to describe these stages and product layer diffusion was pointed out to be the primary rate-limiting step in both stages. Hence, in order to achieve more efficient P leaching, further attempt is essential, e.g., reducing the thickness or improving the porosity of the product layer, using leaching agents that can effectively penetrate the product layer.

CRediT authorship contribution statement

Tan-Phat Vo: Writing – review & editing, Writing – original draft, Visualization, Methodology, Formal analysis, Data curation, Conceptualization. **Ruichi Zhang:** Writing – review & editing, Methodology, Investigation, Validation. **Jukka Rintala:** Supervision, Conceptualization. **Keke Xiao:** Writing – review & editing. **Chao He:** Writing – review & editing, Supervision, Methodology, Conceptualization, Funding acquisition, Investigation, Resources.

Declaration of competing interest

The authors declare that they have no known competing financial interests or personal relationships that could have appeared to influence the work reported in this paper.

Data availability

No data was used for the research described in the article.

Acknowledgements

We acknowledge the financial support from Tampere University, the Academy Research Fellowship and its related research project funded by Research Council of Finland (decision numbers: 341052, 346578).

Appendix A. Supplementary data

Supplementary data to this article can be found online at https://doi.org/10.1016/j.wasman.2024.09.004.

References

Aghbashlo, M., Hosseinzadeh-Bandbafha, H., Shahbeik, H., Tabatabaei, M., 2022. The role of sustainability assessment tools in realizing bioenergy and bioproduct systems. Biofuel Res. J. 9, 1697–1706. https://doi.org/10.18331/BRJ2022.9.3.5.

Atienza–Martínez, M., Gea, G., Arauzo, J., Kersten, S.R.A., Kootstra, A.M.J., 2014. Phosphorus recovery from sewage sludge char ash. Biomass and Bioenergy 65, 42–50. Doi: 10.1016/j.biombioe.2014.03.058.

Bouaouda, S., Souabi, S., Bouyakhsass, R., Taleb, A., Madinzi, A., Anouzla, A., 2023. Techniques for treating leachate discharges: a critical review. Euro-Mediterranean Journal for Environmental Integration 8, 573–599. https://doi.org/10.1007/s41207-023-00366-2.

Chanaka Udayanga, W.D., Veksha, A., Giannis, A., Lisak, G., Chang, V.-W.-C., Lim, T.-T., 2018. Fate and distribution of heavy metals during thermal processing of sewage sludge. Fuel 226, 721–744. https://doi.org/10.1016/j.fuel.2018.04.045.

European Commission, Directorate-General for Internal Market, I., Entrepreneurship and SMEs, Grohol, M., Veeh, C., 2023. Study on the critical raw materials for the EU 2023 – Final report. Publications Office of the European Union. Doi: 10.2873/725585.

Donatello, S., Tong, D., Cheeseman, C.R., 2010. Production of technical grade phosphoric acid from incinerator sewage sludge ash (ISSA). Waste Manag. 30, 1634–1642. https://doi.org/10.1016/j.wasman.2010.04.009.

Du, C., Gao, X., Ueda, S., Kitamura, S., 2020. A kinetic study on selective leaching of phosphorus from dephosphorization slag. Journal of Sustainable Metallurgy 6, 724–738. https://doi.org/10.1007/s40831-020-00309-z.

Elzinga, E.J., Sparks, D.L., 2007. Phosphate adsorption onto hematite: An in situ ATR-FTIR investigation of the effects of pH and loading level on the mode of phosphate surface complexation. J. Colloid Interface Sci. 308, 53–70. https://doi.org/10.1016/j.jcis.2006.12.061.

Fan, J., Li, Y., Yu, H., Li, Y., Yuan, Q., Xiao, H., Li, F., Pan, B., 2020. Using sewage sludge with high ash content for biochar production and Cu(II) sorption. Sci. Total Environ. 713, 136663 https://doi.org/10.1016/j.scitotenv.2020.136663.

Fang, L., Li, J., Guo, M.Z., Cheeseman, C.R., Tsang, D.C.W., Donatello, S., Poon, C.S., 2018. Phosphorus recovery and leaching of trace elements from incinerated sewage sludge ash (ISSA). Chemosphere 193, 278–287. https://doi.org/10.1016/j.chemosphere.2017.11.023.

Faraji, F., Alizadeh, A., Rashchi, F., Mostoufi, N., 2022. Kinetics of leaching: a review. Rev. Chem. Eng. 38, 113–148. https://doi.org/10.1515/revce-2019-0073.

Gao, N., Kamran, K., Quan, C., Williams, P.T., 2020. Thermochemical conversion of sewage sludge: a critical review. Prog. Energy Combust. Sci. 79, 100843 https://doi.org/10.1016/j.pecs.2020.100843.

He, C., Zhao, J., Yang, Y., Wang, J.-Y., 2016. Multiscale characteristics dynamics of hydrochar from hydrothermal conversion of sewage sludge under sub-and near-critical water. Bioresour. Technol. 211, 486–493. https://doi.org/10.1016/j.biortech.2016.03.110.

Ho, Y.-S., Harouna-Oumarou, H.A., Fauduet, H., Porte, C., 2005. Kinetics and model building of leaching of water-soluble compounds of Tilia sapwood. Sep. Purif. Technol. 45, 169–173. https://doi.org/10.1016/j.seppur.2005.03.007.

Hu, S., Yi, K., Li, C., Ma, S., Liu, J., Yang, W., 2023. Efficient and selective recovery of iron phosphate from the leachate of incinerated sewage sludge ash by thermally induced precipitation. Water Res. 238, 120024 https://doi.org/10.1016/j.watres.2023.120024.

Januševičius, T., Mažeikienė, A., Danila, V., Paliulis, D., 2022. The characteristics of sewage sludge pellet biochar prepared using two different pyrolysis methods. Biomass Convers. Biorefin. https://doi.org/10.1007/s13399-021-02295-y.

Jupp, A.R., Beijer, S., Narain, G.C., Schipper, W., Slootweg, J.C., 2021. Phosphorus recovery and recycling–closing the loop. Chemical Society Reviews 50, 87–101. https://doi.org/DOI Doi: 10.1039/D0CS01150A.

Kan, T., Strezov, V., Evans, T., 2016. Effect of the Heating Rate on the thermochemical behavior and biofuel properties of sewage sludge pyrolysis. Energy Fuels 30, 1564–1570. https://doi.org/10.1021/acs.energyfuels.5b02232.

Kleemann, R., Chenoweth, J., Clift, R., Morse, S., Pearce, P., Saroj, D., 2017. Comparison of phosphorus recovery from incinerated sewage sludge ash (ISSA) and pyrolysed sewage sludge char (PSSC). Waste Manag. 60, 201–210. https://doi.org/10.1016/j.wasman.2016.10.055.

Lamastra, L., Suciu, N.A., Trevisan, M., 2018. Sewage sludge for sustainable agriculture: contaminants' contents and potential use as fertilizer. Chemical and Biological Technologies in Agriculture 5, 1–6. https://doi.org/10.1186/s40538-018-0122-3.

Lee, M., Kim, D.-J., 2017. Identification of phosphorus forms in sewage sludge ash during acid pre-treatment for phosphorus recovery by chemical fractionation and spectroscopy. J. Ind. Eng. Chem. 51, 64–70. https://doi.org/10.1016/j.jiec.2017.02.013.

Li, Z., Xie, Z., Deng, J., He, D., Zhao, H., Liang, H., 2021. Leaching Kinetics of Rare Earth Elements in Phosphoric Acid from Phosphate Rock. Metals 11. https://doi.org/10.3390/met11020239.

Liang, S., Chen, H., Zeng, X., Li, Z., Yu, W., Xiao, K., Hu, J., Hou, H., Liu, B., Tao, S., Yang, J., 2019. A comparison between sulfuric acid and oxalic acid leaching with subsequent purification and precipitation for phosphorus recovery from sewage sludge incineration ash. Water Res. 159, 242–251. https://doi.org/10.1016/j.watres.2019.05.022.

Lin, R., Ritz, G.P., 1993. Studying individual macerals using ir microspectrometry, and implications on oil versus gas/condensate proneness and "low-rank" generation. Org Geochem. 20, 695–706. https://doi.org/10.1016/0146-6380(93)90055-GPhosphorus.

Liu, H., Hu, G., Basar, I.A., Li, J., Lyczko, N., Nzihou, A., Eskicioglu, C., 2021a. Phosphorus recovery from municipal sludge-derived ash and hydrochar through wet-chemical technology: A review towards sustainable waste management. Chem. Eng. J. 417, 129300 https://doi.org/10.1016/j.cej.2021.129300.

Liu, R., Long, Y., Zhou, Y., Liu, Z., Liu, X., Huo, X., Xie, Z., Tao, C., 2021b. Rigid-Flexible Combined Impeller Enhancement in Leaching of Phosphate Rock: a Kinetics Study. ACS Omega 6, 33206–33214. https://doi.org/10.1021/acsomega.1c05836.

Liu, H., Lyczko, N., Nzihou, A., Eskicioglu, C., 2023. Phosphorus recovery from municipal sludge-derived hydrochar: Insights into leaching mechanisms and hydroxyapatite synthesis. Water Res. 241, 120138 https://doi.org/10.1016/j.watres.2023.120138.

Lu, H., Zhang, W., Wang, S., Zhuang, L., Yang, Y., Qiu, R., 2013. Characterization of sewage sludge-derived biochars from different feedstocks and pyrolysis temperatures. J. Anal. Appl. Pyrol. 102, 137–143. https://doi.org/10.1016/j.jaap.2013.03.004.

Lv, N., Su, C., Kong, H., Wang, H., Dong, Y., 2022. Leaching process of phosphorus and iron from steelmaking slag into malic acid solution. J. Iron Steel Res. Int. 29, 951–960. https://doi.org/10.1007/s42243-021-00663-6.

Meng, X., Huang, Q., Xu, J., Gao, H., Yan, J., 2019. A review of phosphorus recovery from different thermal treatment products of sewage sludge. Waste Disposal & Sustainable Energy 1, 99–115. https://doi.org/10.1007/s42768-019-00007-x.

Merzari, F., Goldfarb, J., Andreottola, G., Mimmo, T., Volpe, M., Fiori, L., 2020. Hydrothermal carbonization as a strategy for sewage sludge management: influence of process withdrawal point on hydrochar properties. Energies 13. https://doi.org/10.3390/en13112890.

Mew, M., 2016. Phosphate rock costs, prices and resources interaction. Sci. Total Environ. 542, 1008–1012. https://doi.org/10.1016/j.scitotenv.2015.08.045.

Pérez, C., Boily, J.-F., Skoglund, N., Jansson, S., Fick, J., 2022. Phosphorus release from hydrothermally carbonized digested sewage sludge using organic acids. Waste Manag. 151, 60–69. https://doi.org/10.1016/j.wasman.2022.07.023.

Petzet, S., Peplinski, B., Cornel, P., 2012. On wet chemical phosphorus recovery from sewage sludge ash by acidic or alkaline leaching and an optimized combination of both. Water Res. 46, 3769–3780. https://doi.org/10.1016/j.watres.2012.03.068.

Qiang, L., Bai, B., Peng, Z., Zhang, S., Chang, H., Sun, M., Xu, L., Ma, X., 2021. Research on the relationship between the structure and pyrolysis characteristics of pretreated Shendong coal. Fuel 305, 121515. https://doi.org/10.1016/j.fuel.2021.121515.

Ray, H.S., Ray, S., 2018. Diffusion Through Product Layer. In: Ray, H.S., Ray, S. (Eds.), Kinetics of Metallurgical Processes. Springer Singapore, Singapore, pp. 83–118. https://doi.org/10.1007/978-981-13-0686-0_4.

Shiba, N.C., Ntuli, F., 2017. Extraction and precipitation of phosphorus from sewage sludge. Waste Manag. 60, 191–200. https://doi.org/10.1016/j.wasman.2016.07.031.

Stark, K., Plaza, E., Hultman, B., 2006. Phosphorus release from ash, dried sludge and sludge residue from supercritical water oxidation by acid or base. Chemosphere 62, 827–832. https://doi.org/10.1016/j.chemosphere.2005.04.069.

Suggate, R., Dickinson, W., 2004. Carbon NMR of coals: the effects of coal type and rank. Int. J. Coal Geol. 57, 1–22. https://doi.org/10.1016/S0166-5162(03)00116-2.

Tang, Y., Alam, M.S., Konhauser, K.O., Alessi, D.S., Xu, S., Tian, W., Liu, Y., 2019. Influence of pyrolysis temperature on production of digested sludge biochar and its application for ammonium removal from municipal wastewater. J. Clean. Prod. 209, 927–936. https://doi.org/10.1016/j.jclepro.2018.10.268.

Vogel, C., Kohl, A., Adam, C., 2011. Spectroscopic investigation in the mid- and far-infrared regions of phosphorus fertilizers derived from thermochemically treated sewage sludge ash. Appl. Spectrosc. 65, 265–271. https://doi.org/10.1366/10-06168.

Waldmüller, W., Herdzik, S., Gaderer, M., 2021. Combined filtration and oxalic acid leaching for recovering phosphorus from hydrothermally carbonized sewage sludge. J. Environ. Chem. Eng. 9, 104800 https://doi.org/10.1016/j.jece.2020.104800.

Wang, X., Chi, Q., Liu, X., Wang, Y., 2019. Influence of pyrolysis temperature on characteristics and environmental risk of heavy metals in pyrolyzed biochar made

from hydrothermally treated sewage sludge. Chemosphere 216, 698–706. https://doi.org/10.1016/j.chemosphere.2018.10.189.

Wang, Q., Li, J., Tang, P., Fang, L., Poon, C.S., 2018. Sustainable reclamation of phosphorus from incinerated sewage sludge ash as value-added struvite by chemical extraction, purification and crystallization. J. Clean. Prod. 181, 717–725. https://doi.org/10.1016/j.jclepro.2018.01.254.

Wang, J., Zhuang, X., Kong, J., Liu, Y., Du, X., Luo, X., Xing, P., 2017. Kinetics analysis of leaching phosphorus from rice husk ash assisted by ultrasound. Sep. Sci. Technol. 52, 1265–1274. https://doi.org/10.1080/01496395.2017.1287198.

Wei, F., Liao, J., Chang, L., Han, Y., Bao, W., 2019. Transformation of functional groups during lignite heat-treatment and its effects on moisture re-adsorption properties. Fuel Process. Technol. 192, 210–219. https://doi.org/10.1016/j.fuproc.2019.04.028.

Yang, X., Wang, B., Guo, Y., Yang, F., Cheng, F., 2023. Insights into the structure evolution of sewage sludge during hydrothermal carbonization under different temperatures. J. Anal. Appl. Pyrol. 169, 105839 https://doi.org/10.1016/j.jaap.2022.105839.

Yu, X., Nakamura, Y., Otsuka, M., Omori, D., Haruta, S., 2021. Development of a novel phosphorus recovery system using incinerated sewage sludge ash (ISSA) and phosphorus-selective adsorbent. Waste Manag. 120, 41–49. https://doi.org/10.1016/j.wasman.2020.11.017.

Zhang, T., He, X., Deng, Y., Tsang, D.C.W., Jiang, R., Becker, G.C., Kruse, A., 2020. Phosphorus recovered from digestate by hydrothermal processes with struvite crystallization and its potential as a fertilizer. Sci. Total Environ. 698, 134240 https://doi.org/10.1016/j.scitotenv.2019.134240.

Zhuang, X., Zhan, H., Song, Y., He, C., Huang, Y., Yin, X., Wu, C., 2019. Insights into the evolution of chemical structures in lignocellulose and non-lignocellulose biowastes during hydrothermal carbonization (HTC). Fuel 236, 960–974. https://doi.org/10.1016/j.fuel.2018.09.019.